ELSEVIER

Journal of Alloys and Compounds 281 (1998) 12–16

Journal of ALLOYS AND COMPOUNDS

A magnetic and compositional study of the disproportionated stage of the solid-HDDR process in NdFeB-type materials

P. Thompson[a,*], O. Gutfleisch[b], J.N. Chapman[a], I.R. Harris[b], W.A.P. Nicholson[a]

[a]*Department of Physics and Astronomy, University of Glasgow, Glasgow G12 8QQ, UK*
[b]*School of Metallurgy and Materials, University of Birmingham, Birmingham B15 2TT, UK*

Abstract

A thinned sample of $Nd_{12.8}Fe_{69.2}Co_{11}Ga_1B_6$ after the disproportionation stage of the solid-HDDR process has been examined using advanced transmission electron microscopy techniques. High resolution X-ray mapping is particularly useful for showing the distribution of all elements with the exception of B. Elemental maps show clearly that during the disproportionation reaction, Co and Ga partitioned into the α-Fe and not into the NdH_2. Domain observations using Lorentz microscopy revealed irregular domain walls whose location was influenced by the non-magnetic NdH_2 inclusions. The walls moved easily under small applied magnetic fields in a series of discrete jumps. The behaviour was consistent with that of a soft magnetic material with low anisotropy, and differed markedly from that of the recombined material.

Keywords: Disproportionated phase; HDDR; Lorentz electron microscopy; NdFeB; X-ray mapping

1. Introduction

The hydrogenation disproportionation desorption recombination (HDDR) process [1,2] is well known as a method of grain refinement that can produce highly coercive isotropic and anisotropic [3] powders. Despite extensive study, the mechanism of inducement of magnetic anisotropy is not yet fully understood [4]. The key to the solution probably lies in the intermediate disproportionated stage of the process. There have been many transmission electron microscopy (TEM) studies of this material [5–9] and here we extend such studies by high resolution X-ray mapping and Lorentz microscopy. We have previously studied the magnetic domain structure and how it relates to the crystallography of the recombined solid-HDDR processed NdFeB-type material [10]. The present work offers the possibility of gaining a more complete description from both compositional and micromagnetic standpoints of the all important intermediate stage.

The material studied was an alloy of composition $Nd_{12.8}Fe_{69.2}Co_{11}Ga_1B_6$ which had been homogenised at 1100°C for 20 h in an argon atmosphere. It was heated under vacuum to 830°C and a hydrogen pressure of 10^5 Pa was then introduced for 60 min to disproportionate the sample (solid-HDDR process [11]). The processing was interrupted after the disproportionation stage where previous studies had shown the sample to be predominantly composed of $NdH_{2\pm x}$, α-Fe and Fe_2B, formed by the reaction of $Nd_2Fe_{14}B$ with hydrogen under the stated conditions. The fully disproportionated material was subsequently polished and ion beam thinned until electron transparent (<100 nm thick). All the TEM observations were made using a modified Philips CM20 FEG microscope optimised for the study of magnetic materials [12].

In the following section we describe the X-ray mapping technique after which maps are presented showing typical elemental distributions. Thereafter, Lorentz microscopy is used to show the domain processes in the predominant α-Fe phase.

2. Nanocompositional studies

In previous work [6,7] spot X-ray analyses have been used to obtain the composition of a local area. However, to get a good statistical spread of analyses is laborious. X-ray mapping reduces the chance of observer bias and enables the compositional variations of an area to be visualised easily. Uehara et al. [13] collected X-ray maps of a large

*Corresponding author. Current address: Department of Geology and Geophysics, University of Edinburgh, West Mains Road, Edinburgh EH9 3JW, UK. Fax: +44-131-668-3184; e-mail: pauline.thompson@glg.ed.ac.uk

0925-8388/98/$ – see front matter
PII: S0925-8388(98)00762-2

undecomposed $Nd_2Fe_{14}B$ grain using an electron microprobe. In the electron microprobe the resolution of the analysis is determined by the volume within the sample excited by the incident electron beam rather than by the electron beam diameter itself. The distribution is tear-drop shaped and often exceeds 1 μm in diameter at its maximum extent. This is clearly of limited use when finely divided features on a scale of 50 nm or less are present as is the case here. In thin TEM samples much higher resolution can be achieved as beam spreading is restricted to the neck of the tear drop. Details of how both the size of the electron probe and beam spreading in a thin sample affect the overall resolution obtainable have been given elsewhere [14]. However, whilst resolutions on the scale of 2 to 4 nm can be achieved under realistic experimental conditions, the efficiency of X-ray production is low in thinned samples and hence collection times are inevitably long. The situation is further exacerbated if the distribution of trace elements is of interest. In practice, an instrument with a high brightness electron source is a prerequisite for experiments of this kind and our instrument is equipped with a thermally-assisted field emission gun. Further requirements are stable emission over collection periods which can be up to 1 h and low drift of both the specimen stage and the electronic circuitry controlling the position of the probe itself.

A typical X-ray spectrum of the disproportionated material is shown in Fig. 1. The spectrum was collected

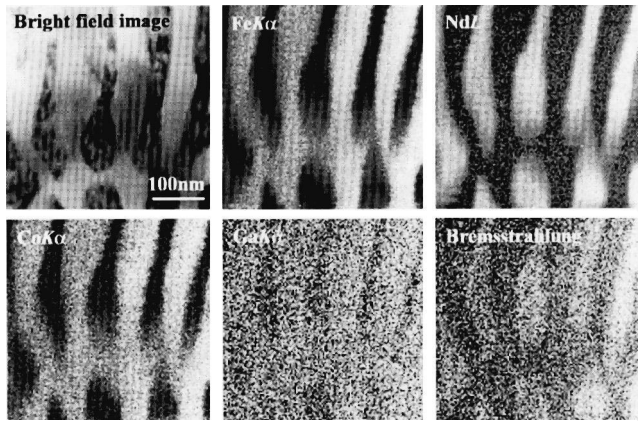

Fig. 2. Bright field image and corresponding X-ray maps of a fine rod-like area of the disproportionated material (dwell time 100 ms per pixel).

over a broad region, 1.5 μm in diameter, of the finer grained rod-like material (see, for example, Fig. 2a). A spectrum taken from the coarser regions (see, for example, Fig. 3a) had a very similar bulk composition. For mapping, a focused electron probe of approximate diameter 3 nm and carrying a current of 1 nA was used. The maps were 128×128 pixels with step sizes between adjacent pixels being ≥3 nm. Pixel dwell times of 50 or 100 ms gave a convenient compromise between adequate statistical accuracy and excessive total acquisition time.

Fig. 1 shows, shaded in black, the windows used in the

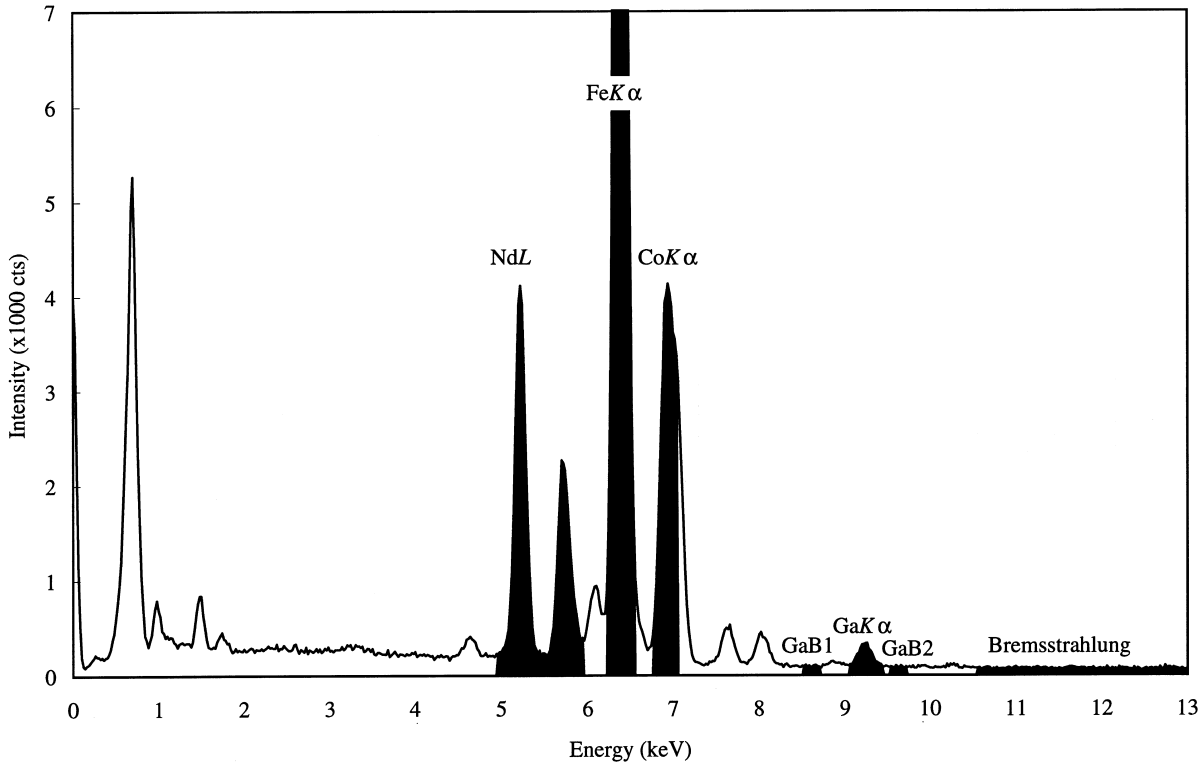

Fig. 1. X-ray spectrum of broad area of a fine grained region of the sample showing the windows used for collection of the signals for X-ray mapping in black (count time 100 s).

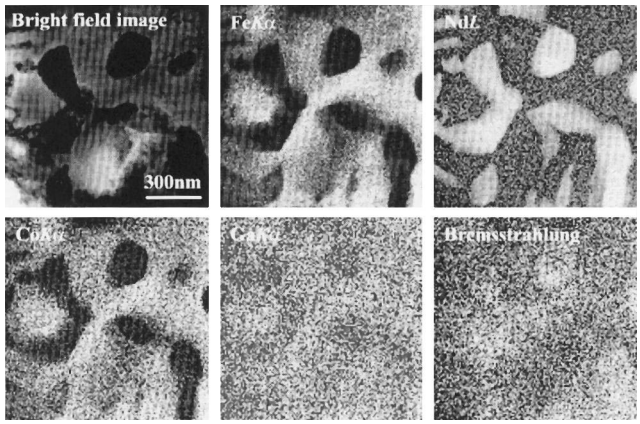

Fig. 3. Bright field image and corresponding X-ray maps of a coarse area of the disproportionated material (dwell time 50 ms per pixel).

mapping experiments. A number of considerations must be borne in mind to obtain reliable maps for all the elements of interest. The collection of a Ga signal is particularly difficult as the signal-to-background ratio is so low. Furthermore, the background (due to the continuous Bremsstrahlung spectrum) varies markedly according to whether the probe is centred on a region containing predominantly α-Fe or NdH_2. This is a consequence of the atomic number dependence of the cross-section for Bremsstrahlung production (see, for example, Ref. [15]). Hence here, unlike the cases for Fe and Nd where background contributions are on average small, background subtraction is essential. This is achieved with the help of local background windows (GaB1 and GaB2) set on either side of the Ga Kα window. The Co signal is also difficult to measure as the window used for the Co Kα is overlapped by the low energy part of the Fe Kβ peak. For calculating the Co maps shown here, we fitted the peaks shown in Fig. 1 to separate Co Kα from Fe Kβ. Using a knowledge of the partition function (for Fe Kα and Fe Kβ), we were able to estimate the number of Fe Kβ counts falling in the combined Co Kα and Fe Kβ window from the Fe Kα intensity. Subtraction of the Fe Kβ counts then left a map attributable to the Co Kα alone.

Figs. 2 and 3 show bright field images and the corresponding X-ray maps for the elements Fe, Nd, Co, Ga and the high energy background. Fig. 2 is an area of the fine rod-like structure with NdH_2 embedded in a matrix of α-Fe and Fig. 3 is a more coarse grained region containing the same phases. Both figures show very similar features. The Co and the Ga both appear to follow closely the distribution of Fe rather than Nd. Whilst the Bremsstrahlung window does not provide additional compositional information it confirms that the background from NdH_2 is indeed greater than from α-Fe and suggests that overall there is some small thickness variation across the field of view. Also worthy of note is the comparative simplicity of the X-ray maps compared with the bright field images. Diffraction contrast in the latter can make it difficult to determine the sizes and shapes of the various phases present; no such problems exist with the X-ray maps. The electron microprobe mapping work of Ref. [13] found undecomposed $Nd_2Fe_{14}B$ whereas, although we did not look exhaustively, we could not find any evidence for such grains. This may be a consequence of the different temperature conditions for disproportionation and the solid-HDDR processing method that we used to manufacture the samples.

3. Domain studies

Fresnel imaging [16] was used to reveal the magnetic domain structure in the thinned samples. In the Fresnel mode domain walls are observed as dark and light narrow bands by simply defocusing the imaging lens. In our Philips CM20 TEM extra (Lorentz) lenses permit observations in field free space while the conventional objective lens can be used to apply a vertical magnetic field to the sample. The applied field experienced in the specimen plane is changed by tilting and rotating the sample.

The magnetic structure of the thermally-demagnetised disproportionated material is difficult to observe and complicated by the presence of the non-magnetic phase (NdH_2) contained within the magnetic matrix of α-Fe. Domain walls can easily be confused with boundaries between magnetic and non-magnetic phases in the Fresnel mode. Furthermore, as domain walls cannot pass through a non-magnetic material the edges of domains frequently lie along the edges of the magnetic grains. In the fine grained material occasional short domain walls can be seen crossing the α-Fe between the NdH_2 grains, whilst in the coarser disproportionated material domain walls can be seen more frequently, although they are strongly influenced by the location of neighbouring NdH_2. Fig. 4a and b show bright field and Fresnel images, respectively, of a coarse region in the thermally demagnetised state. In the Fresnel image a curved domain wall (AA′) can be observed. The domain wall cannot end within the magnetic material (for example, at A or A′) but does go out of contrast if local diffraction conditions are unfavourable. It is apparent that the wall is far from straight, the curvature presumably being partly caused by the presence of the NdH_2 inclusions (e.g., I). The fainter parallel lines running approximately down the length of the image are not magnetic and were probably artefacts introduced during sample preparation.

When a magnetic field was applied to the sample the domain wall movement could be observed in situ and recorded using a low-light-level TV camera and video recorder. In the fine rod-like regions of the sample domain walls were seen to jump between boundaries at fields <20 kA m^{-1}. At higher fields extensive magnetisation realignment took place in adjacent thicker regions leading to a

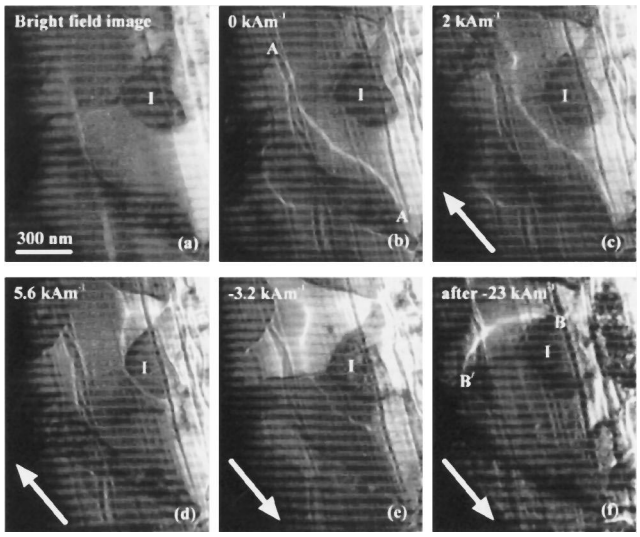

Fig. 4. (a) Bright field image of a coarse region showing an α-Fe matrix surrounding inclusions of NdH_2 (e.g., I); (b) corresponding Fresnel image at zero field showing a domain wall AA′; (c,d) movement of the domain wall under increasing positive fields; (e) movement of the domain wall on reversing the field; (f) remanent state after a larger reverse field had been applied showing a new domain wall BB′.

loss of image (due to the consequent substantial deflection of the electron beam).

In the coarser regions (such as that shown in Fig. 4) it was possible to track the movement of walls more closely. The domain walls in the centres of α-Fe grains tended to move in discrete jumps across the specimen. Fig. 4c and d show the wall AA′ moving under progressively larger positive fields. By a field of 5.6 kA m^{-1} the wall seemed to be held by the inclusion I. When the field was reversed the wall AA′ moved back towards its original position (Fig. 4e). However, on application of a somewhat larger negative field a more profound change took place leading to a wall lying approximately orthogonal to its original direction (BB′ in Fig. 4f). That the change was irreversible was clear in that Fig. 4f is of a remanent state following removal of a reverse field of -23 kA m^{-1}. Examination of low magnification images on video showed that as the reverse field was increased the overall trend was for abrupt jumps of wall orientation through approximately 90° before complete reversal appeared to have occurred. Fields with in-plane components $\approx$30 kA m^{-1} were typically needed.

4. Conclusions

The distribution of elements observed, whereby Co and Ga partition closely with the α-Fe and are substantially absent from the Nd-containing areas in the fully disproportionated material, is consistent with previous work and not particularly surprising in itself. However, Figs. 2 and 3 show that high spatial resolution X-ray mapping is a very efficient way of collecting nanocompositional data without the possibility of introducing the bias in probe positioning that could occur when taking a series of point spectra. Furthermore, the absence of diffraction contrast from X-ray maps makes it easy to identify the sizes and shapes of the different phases present. Although the Ga maps are very noisy, it is encouraging that useful information can still be obtained about the distribution of trace elements whose overall concentration is as low as 1% in an experiment lasting less than 30 min.

Our magnetic observations show that the matrix in the disproportionated phase is basically a soft magnetic phase with properties totally different from those of the recombined material. Although containing both Co and Ga, and being substantially disrupted by the presence of NdH_2 inclusions, the behaviour of the α-Fe is related to that of the epitaxial Fe films studied by Gu et al. [17]. These authors reported domain walls moving in discrete jumps at low fields and reversal frequently involved jumps of 90° in the magnetic alignment, consistent with four-fold in-plane anisotropy. In the disproportionated material walls are much more irregular and are influenced by the non-magnetic inclusions. Fields for reversal are significantly higher but there seems little difference in the basic phenomena encountered.

We conclude that specialist techniques available on advanced TEMs can play an important role in characterising the properties of very complex and inhomogeneous materials such as disproportionated NdFeB-type alloys.

Acknowledgements

We would like to thank Rare Earth Products (UK) who provided the materials and the Engineering and Physical Sciences Research Council who contributed the financial support that enabled this research.

References

[1] T. Takeshita, R. Nakayama, in: Proceedings of the 10th International Workshop on Rare-Earth Magnets and Their Applications, Kyoto, Japan, 1989, p. 551.
[2] P.J. McGuiness, X.J. Zhang, X.J. Yin, I.R. Harris, J. Less-Common Met. 158 (1990) 359.
[3] T. Takeshita, R. Nakayama, in: Proceedings of the 11th International Workshop on Rare-Earth Magnets and Their Applications, Pittsburgh, 1990, p. 49.
[4] O. Gutfleisch, I.R. Harris, J. Phys. D: Appl. Phys. 29 (1996) 2255.
[5] M. Uehara, H. Tomizawa, S. Hirosawa, T. Tomida, Y. Maehara, IEEE Trans. Magn. 29 (1993) 2770.
[6] P. Choi, T. Tomida, Y. Maehara, M. Uehara, S. Hirosawa, in: Proceedings of the 2nd Pacific Rim International Conference on Advanced Materials and Processing, 1995, p. 1401.
[7] T. Tomida, P. Choi, Y. Maehara, M. Uehara, H. Tomizawa, S. Hirosawa, J. Alloys Comp. 242 (1996) 129.
[8] H. Nakamura, R. Suefuji, D. Book, T. Kagotani, S. Sugimoto, M.

Okada, M. Homma, in: 117th Meeting Japanese Institute of Metals, 1995.
[9] O. Gutfleisch, M. Matzinger, J. Fidler, I.R. Harris, J. Magn. Magn. Mater. 147 (1995) 320.
[10] P. Thompson, O. Gutfleisch, J.N. Chapman, I.R. Harris, J. Phys. D: Appl. Phys. 30 (1997) 1854.
[11] O. Gutfleisch, N. Martinez, M. Verdier, I.R. Harris, J. Alloys Comp. 215 (1994) 227.
[12] J.N. Chapman, L.J. Heyderman, S. McVitie, W.A.P. Nicholson, in: Y. Bando, M. Kamo, H. Haneda, T. Aizawa (Eds.), Proceedings of the 2nd International Symposium on Advanced Materials (ISAM'95), 1995, p. 123.
[13] M. Uehara, P. Choi, T. Tomida, H. Tomizawa, S. Hirosawa, Y. Maehara, IEEE Trans. Magn. 31 (1995) 3632.
[14] A.J. McGibbon, J.N. Chapman, A.G. Cullis, N.G. Chew, S.J. Bass, L.L. Taylor, J. Appl. Phys. 65 (1989) 2293.
[15] H.W. Koch, J.W. Motz, Rev. Mod. Phys. 31 (1959) 920.
[16] J.N. Chapman, J. Phys. D: Appl. Phys. 17 (1984) 623.
[17] E. Gu, A.C. Bland, C. Daboo, M. Gester, L.M. Brown, R. Ploessl, J.N. Chapman, Phys. Rev. B 51 (1995) 3596.